Electronic structure and thermoelectric properties of layered PbSe-WSe_2 materials

Lijun Zhang and D. J. Singh
Materials Science and Technology Division, Oak Ridge National Laboratory, Oak Ridge, Tennessee 37831-6114, USA
(Received 11 June 2009; published 20 August 2009)

The first members of the series of intergrowth PbSe-WSe_2 compounds are investigated using first-principles electronic-structure calculations and Boltzmann transport theory. These materials are moderate band-gap semiconductors. The valence-band edges are primarily derived from PbSe-derived states while the conduction bands have mixed PbSe-WSe_2 character. The transport calculations show that high thermopowers are attainable at moderate to high p-type doping levels, consistent with good thermoelectric performance at temperatures from 300 to 1000 K.

DOI: 10.1103/PhysRevB.80.075117 PACS number(s): 72.20.Pa, 71.20.Nr

I. INTRODUCTION

Thermoelectric materials for waste-heat recovery are the subject of considerable recent interest that derives from efforts to improve energy efficiency and reduce CO_2 emissions. A particularly promising application is the recovery of energy from the exhaust gas of vehicles. In conventional vehicles driven by internal combustion engines approximately one third of the energy content of the fuel is dissipated as waste heat in the exhaust gas stream and this dissipation is at sufficiently high temperatures that well over half of this dissipation could in principle be recovered, based on thermodynamic limits. Considering that only approximately one third or less of the energy from fuel is used to actually drive vehicles and their accessories (the remainder is dissipated due to drive train friction or in radiated heat from the engine and coolant), there are very significant potential-energy savings from exhaust gas waste-heat recovery. Thermoelectrics offer a promising way to recover energy from this waste heat. However the efficiency of present thermoelectric generators is much lower than the thermodynamic Carnot limit, primarily because of limitations in presently known thermoelectric materials.[1–3]

The key material parameter related to efficiency is the dimensionless figure of merit, $ZT=\sigma S^2 T/\kappa$, where σ is the electrical conductivity, S is the thermopower, and $\kappa=\kappa_e+\kappa_l$ is the thermal conductivity composed of electronic and lattice parts.[4,5] ZT averaged over the operating temperature range and over the p- and n-type thermoelectric legs defines the maximum efficiency that can be obtained using given materials, with $ZT=\infty$ corresponding to Carnot efficiency. It is important to note that the electronic thermal and electrical conductivities, κ_e and σ are connected by the Wiedemann-Franz relation, $\kappa_e=L\sigma T$. This means that $ZT=rS^2/L$, with $r=(\kappa_e)/(\kappa_l+\kappa_e)<1$, and as such, with the normal value of the Lorenz constant, $ZT=1$ requires a minimum $S\sim160\ \mu\mathrm{V/K}$. Thus thermoelectric performance imposes a dual requirement: (1) high S and (2) low-lattice thermal conductivity on the scale of the electronic thermal conductivity (i.e., high r). By far the most common strategy for optimizing materials considering this dual requirement has been to focus on semiconductors with heavy band masses, and as high mobility as possible, and then to concentrate on lowering thermal conductivity, optimizing the carrier concentration to find the best balance between electrical conductivity and thermopower.

PbTe and PbTe-based thermoelectrics are of particular interest for thermoelectric generators operating at temperatures appropriate for exhaust waste-heat recovery.[5] Furthermore, recent developments such as the LAST phases (PbTe with the addition of Ag_xSbTe_2),[6] and resonantly enhanced Tl-doped PbTe,[7] both of which have ZT well above unity, suggest that PbTe-based materials may offer performance better than any other materials for this application.

In spite of its simple rock-salt-type crystal structure, PbTe shows a combination of heavy-band masses, low-thermal conductivity, and high mobility that favors thermoelectric performance. In particular, optimized samples with both high S and high values of r in the appropriate temperature range (100–500 °C) can be synthesized. The high performance of PbTe-based materials relative to other materials with small unit cells and simple crystal structures is thought to be related to the relatively similar electronegativities of Pb and Te (favoring high mobility), the heavy-mass elements,[5,8] and soft phonons associated with nearness to ferroelectricity.[9] Unfortunately, Te is a rare element, and in fact most of the world supply of Te comes as a byproduct of certain types of Cu production. Consequently, large scale use of PbTe-based thermoelectric generators in vehicles may be complicated by materials availability issues. Therefore it is of interest to examine PbTe replacements, provided that they have the potential for high ZT. In this regard, the lighter chalcogenide PbSe has also been investigated as a thermoelectric. The properties of PbSe, while reasonable, are inferior to those of PbTe at moderate T. However, PbSe thermoelectrics do show thermopowers comparable to those of similarly prepared PbTe and may be superior at very high T.[10,11] Thus one may focus on the factor r in improving the performance of PbSe, either by improving the mobility or by lowering the lattice-thermal conductivity. The simple rock-salt structure of PbSe would seem to preclude conventional strategies for reducing the thermal conductivity, such as the introduction of rattlers.[12,13] However, nanostructuring[14–17] may be effective.

Recently, Chiritescu and co-workers reported the finding of ultralow thermal conductivities in layered WSe_2 films with disorder in the c axis stacking.[18] Furthermore, films with alternating PbSe and WSe_2 or $MoSe_2$ blocks have also been grown and these films were also shown to have low thermal conductivities (below 0.1 W/m K in the cross-plane

 ©2009 The American Physical Society

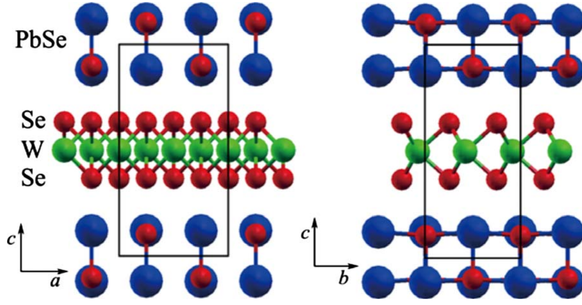

FIG. 1. (Color online) Optimized approximant structure of layered $(PbSe)_m(WSe_2)_n$ ($m=1$ and $n=1$) used in the calculations (see text). Se atoms are denoted as smaller red spheres, Pb as blue, and W as green spheres. The resulting unit cell is orthorhombic containing four $(PbSe)_1(WSe_2)_1$ formula units. Views along different directions are shown, where the c axis represents PbSe and WSe_2 layers stacking directions, a axis corresponds to [100] direction of both subsystems and the b axis is perpendicular to a axis.

direction and ~0.4 W/mK in the in-plane direction).[19–22] However, less is known about the electrical-transport properties. Here we report density-functional investigations of the electronic and electrical-transport properties of these materials. We find that with p-type doping high thermopowers associated with the PbSe layers are obtained at moderate doping levels.

II. STRUCTURE

Bulk WSe_2 occurs in a layered hexagonal structure, lattice parameters $a=3.282$ Å and $c=12.96$ Å,[23] while PbSe occurs in a cubic rock-salt structure, $a=6.121$ Å. Therefore the ratio of the cubic lattice parameter of PbSe to the a lattice parameter of WSe_2 is 1.865, which is intermediate between the values $\sqrt{3}$ and 2, which correspond to an orthorhombic net on the hexagonal lattice. This is consistent with the formation of incommensurate misfit structures in intergrowth compounds, as observed experimentally.[24] A series of such compounds, $(PbSe)_m(WSe_2)_n$ [experimentally characterized as $[(PbSe)_{0.99}]_m(WSe_2)_n$ (Ref. 19)] can be synthesized. These consist of alternating stacks of m layers of rock-salt PbSe and n hexagonal WSe_2 units, along the c-axis direction. Within the planes, the two sublattices are incommensurately modulated along the a axis ([100] direction of both sublattices) and orthogonal b direction with small misfit parameters.

In order to perform electronic-structure calculations it is necessary to use commensurate approximant structures. For this purpose, we note that PbSe is a softer material than WSe_2. Accordingly, we construct approximate structures based on the experimental a lattice parameter of WSe_2, as shown in Fig. 1 for the $m=n=1$ case. This leads to an orthorhombic unit cell. The internal atomic coordinates in these cells were then relaxed using total-energy minimization. This amounts to a strain of +0.07 and −0.07 in the PbSe layer along the a and b crystallographic axes relative to an average experimental $a=6.163$ Å, which is slightly larger than the bulk lattice parameter of PbSe. For this purpose we used the experimental lattice parameter from experiments on the films, $a=6.586$ Å and $b=\sqrt{3}a/2=5.704$ Å, which differs slightly from the reported bulk WSe_2 value. The resulting cells contain four formula units. As mentioned, this construction introduces an orthorhombic in-plane strain, in the softer PbSe layers, which is consistent with structural data for other misfit-layered chalcogenides as evidenced by the unequal a and b lattice parameters that are observed.[24] The out-of-plane lattice parameter, c was set to the sum of experimental sublattice values (6.14 Å and 6.55 Å per unit for PbSe and WSe_2, respectively). We find only moderate $a-b$ anisotropy of the calculated transport properties. This supports the use of the approximant structure.

III. ELECTRONIC-STRUCTURE METHODOLOGY

As noted, the internal atomic coordinates were optimized by total-energy minimization. This was done using the generalized gradient approximation (GGA) of Perdew, Burke, and Ernzerhof (PBE),[25] with the projector augmented wave (PAW) method as implemented in the VASP code.[26,27] A kinetic-energy cutoff of 350 eV was employed and the Hellmann-Feynman forces acting on atoms were relaxed to less than 0.01 eV/Å. After the optimization, the PbSe layers show small distortions (see Fig. 1), e.g., along c direction the Pb atoms slightly approach WSe_2 layers, presumably as a result of interactions with the Se atoms in WSe_2 layers.

The electronic band structures and density of states (DOS) were calculated within the PBE GGA. using general-potential linearized augmented plane-wave (LAPW) method,[28] as implemented in the WIEN2K code.[29] For this purpose the relaxed structures as obtained from the PAW calculation were employed. Both the valence and core states were treated self-consistently. For the valence states we did both scalar relativistic calculations and calculations with spin orbit. The core states were treated fully relativistically. LAPW sphere radii of $2.1a_0$ for Se and $2.3a_0$ for Pb and W were used. We employed converged basis sets plus local orbitals determined by $R_{Se}k_{max}=8.0$, where k_{max} is the plane-wave cutoff in the interstitial region, and R_{Se} is the LAPW sphere radius of Se (the smallest sphere in the present calculations). The temperature and doping-level dependence of thermopower was calculated based on Boltzmann transport theory within the constant scattering-time approximation, using the BOLTZTRAP program.[30] This program evaluates transport coefficients using Boltzmann transport equations (see "Thermopower," below) using band structures from first-principles calculations.

Transport properties can be very sensitive to the Brillouin-zone sampling. We checked convergence and found that sets of approximately 20 000 [for $(PbSe)_1(WSe_2)_1$] and 15 000 [$(PbSe)_2(WSe_2)_1$] nonshifted **k** points were adequate for obtaining well-converged thermopowers in the temperature range above 300 K. We show scalar relativistic band structures because these are simpler and capture the salient features of the full relativistic calculations. All the transport calculations shown were based on the relativistic band structures, including spin-orbit.

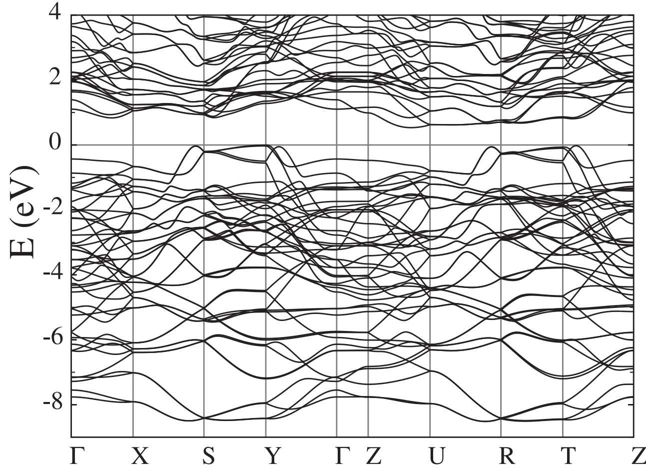

FIG. 2. Calculated scalar relativistic band structure of the $(PbSe)_1(WSe_2)_1$ intergrowth compound. The energy zero is set to the valence-band edge. The lowest bands shown are from the Pb *s* states. The Se *s* bands are at higher binding energy and are not shown.

IV. ELECTRONIC STRUCTURE AND DOPING

We begin with the $m=n=1$ compound. The calculated band structure and electronic DOS for $(PbSe)_1(WSe_2)_1$ are shown in Figs. 2 and 3, respectively. The bands near the valence-band maximum (VBM) originate from the PbSe layers and are of mixed Pb *p* and Se *p* characters. Among these bands near VBM, there are relatively heavy bands with large effective mass at Y and T points that would contribute to high thermopower. This may be seen in the weak dispersion of the top bands along S-Y and R-T. We note that these lines are along the in-plane k_y direction. One may also note that there are also low-dispersion bands in the equivalent k_x directions but these bands are at higher binding energy. In addition to these heavy bands, there are lighter bands along the X-S, Y-Γ, U-R, and T-Z directions. This combination of light and heavy bands is often favorable for thermoelectric materials, since it helps in obtaining a combination of reasonable mobility and high thermopower, as in La-Te thermoelectrics[31] and filled *p*-type skutterudites.[32] This also contributes to a high DOS near the band edge. This is different from bulk PbSe (see below), which has lighter bands near the VBM followed by heavier bands at somewhat higher binding energy. This difference reflects the reduced dimensionality of the PbSe layers in the present case, which reduces the dispersion of the lighter bands. This is also favorable for higher thermopower, as was discussed in general by Hicks and Dresselhaus.[33]

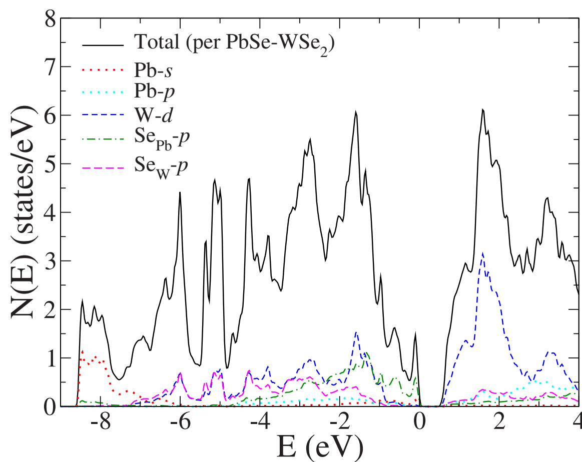

FIG. 3. (Color online) Scalar relativistic Electronic density of states and orbital projections onto the LAPW spheres for $(PbSe)_1(WSe_2)_1$. The projections are on a per atom basis.

TABLE I. Calculated band gaps for $(PbSe)_m(WSe_2)_1$, $m=1,2$, and bulk PbSe with the PBE GGA including spin orbit (SO) and in a scalar relativistic calculation (SR).

Compound	SR(eV)	SO (eV)
Bulk PbSe	0.32	0.07
$m=1$	0.54	0.43
$m=2$	0.44	0.20

The low-lying valence bands around −8.0 eV mainly come from Pb *s* states. The contribution of the WSe_2 sublattice to the valence bands is mainly in the energy range of −7.0 to −1.0 eV with respect to the VBM, where strongly hybridized W *d* and Se *p* states are found. Turning to the conduction bands, the lowest lying conduction bands are heavy and mainly composed of W *d* states. Generally, these heavy bands are expected to contribute to a large thermopower but small carrier mobility. The band gap is indirect, $E_g=0.54$ eV in a scalar relativistic approximation and 0.43 eV with spin orbit (see Table I), with the VBM is located at Y point and the conduction-band minimum (CBM) along Z-U line (also see the top of Fig. 7). We also calculated the electronic structure for bulk PbSe and WSe_2, (Figs. 4–6) and obtained results very similar to previous calculations.[34–36] We note that the electronic structure for the intergrowth compound is similar to what one would obtain by overlapping the electronic structures of the components with an energy shift, at least as far as the main features are concerned. This indicates that the interlayer interactions are moderate.

Doping with mobile carriers is essential for thermoelectric performance. In order to assess the prospects for doping the intergrowth compound we begin by evaluating the doping dependence of the electronic structure using a virtual-crystal approximation based on varying the nuclear charge on the Pb site. This is a beyond rigid-band approximation for doping in the PbSe layers. Figure 7 shows the band structures for doping levels of 0.1 hole (*p* type) and 0.1 electron (*n* type) per PbSe unit, in comparison with the undoped case. We find that the virtual-crystal band structure for *p*-type doping is very similar to the original band structure with a shift of the Fermi energy, i.e., the virtual-crystal and rigid-band pictures are similar. As may be seen, this is not the case for *n*-type doping. In particular, the relative positions of low-lying conduction bands change significantly and the bandgap increases to 0.79 eV with 0.1 electron per PbSe *n*-type doping. This different behavior upon *p*-type or *n*-type dopings reflects the different band character of the VBM and CBM states. In

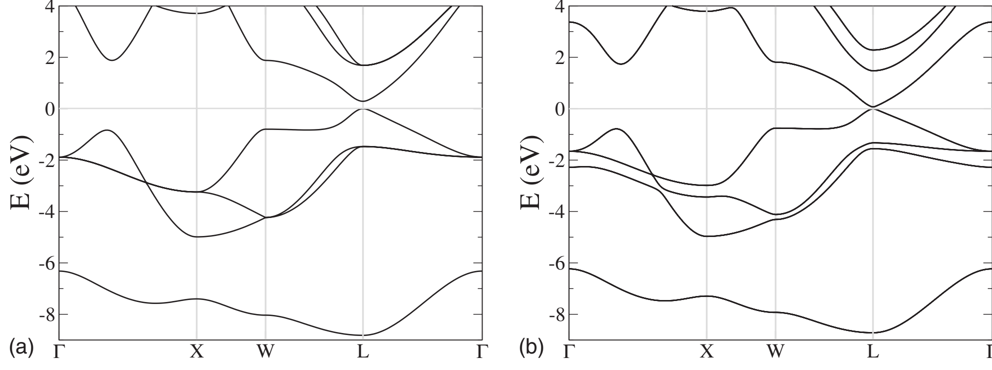

FIG. 4. GGA band structure of PbSe in a scalar relativistic approximation (left) and including spin orbit (right).

general, non-rigid-band behavior implies stronger scattering, which is detrimental to the conductivity. In addition, the mixed $PbSe/WSe_2$ character of the band structure at the CBM is also expected to lead to stronger scattering due to the interfaces. Therefore stronger scattering may be expected for electrons than for holes, at least in this $m=n=1$ compound. In the following we focus on p-type doping.

V. THERMOPOWER

As mentioned, we calculated the thermopowers based on Boltzmann theory within the constant scattering-time approximation. We begin with a brief summary of the formalism. Normally, the equations are written in terms of double integration over the Brillouin zone and energy. However, following Ref. 30, we separate the zone integration and write it as a sum over discrete points since this is how it is evaluated from first-principles band structures. In this approach,[30,37] the temperature and doping-level-dependent thermopower $S(T,\mu)$ is obtained from

$$S_{\alpha\beta}=\sum_{\gamma}(\sigma^{-1})_{\alpha\gamma}\nu_{\beta\gamma}, \quad (1)$$

where σ is the electronic conductivity is given by

$$\sigma_{\alpha\beta}(T,\mu)=\frac{1}{\Omega}\int\sigma_{\alpha\beta}(\varepsilon)\left[-\frac{\partial f_{\mu}(T,\varepsilon)}{\partial\varepsilon}\right]d\varepsilon \quad (2)$$

and

$$\nu_{\alpha\beta}(T,\mu)=\frac{1}{eT\Omega}\int\sigma_{\alpha\beta}(\varepsilon)(\varepsilon-\mu)\left[-\frac{\partial f_{\mu}(T,\varepsilon)}{\partial\varepsilon}\right]d\varepsilon. \quad (3)$$

Here the $\varepsilon_{i,\mathbf{k}}$ are the electron-band energies (band index i), f_{μ} is the Fermi distribution function, μ is the chemical potential which depends on doping level and temperature, T, and Ω is the volume. Band-structure calculations are necessarily done on a discrete grid so that the integrals are in practice replaced by summations over discrete **k** points. The essential ingredients are the energy-projected conductivity tensors (transport distributions)

$$\sigma_{\alpha\beta}(\varepsilon)=\frac{1}{N}\sum_{i,\mathbf{k}}\sigma_{\alpha\beta}(i,\mathbf{k})\delta(\varepsilon-\varepsilon_{i,\mathbf{k}}), \quad (4)$$

where we use a notation $1/N$ to account for the normalization of the sum so that it becomes the integral in the limit where the number of grid points becomes dense. These transport distributions can be obtained using the **k**-dependent conductivity tensor

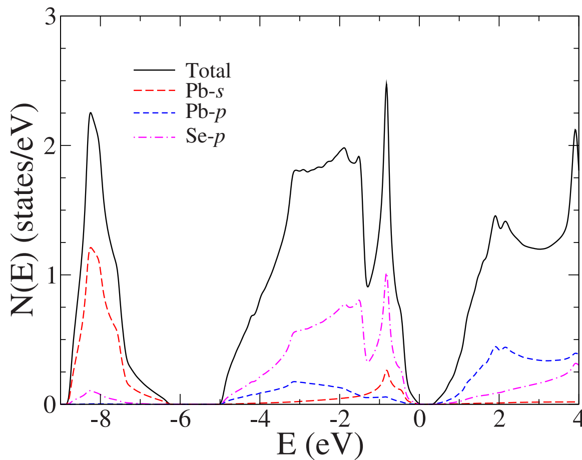

FIG. 5. (Color online) Scalar relativistic electronic density of states and projections for PbSe. Note that the Se p orbitals are spatially extended, and that as a result the projection onto the Se LAPW sphere is proportional to the Se p contribution to the electronic structure but underestimates it.

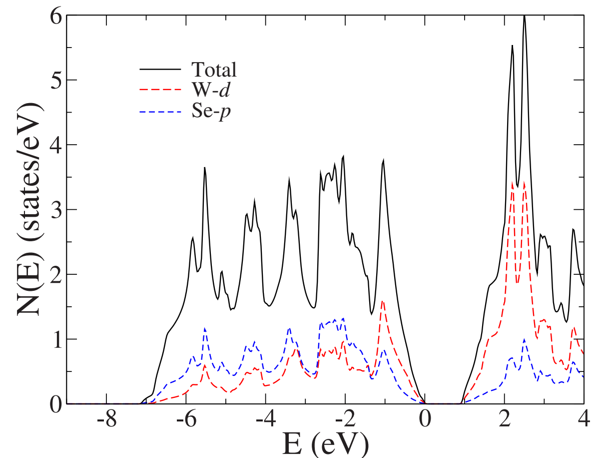

FIG. 6. (Color online) Scalar relativistic electronic density of states and projections for WSe_2.

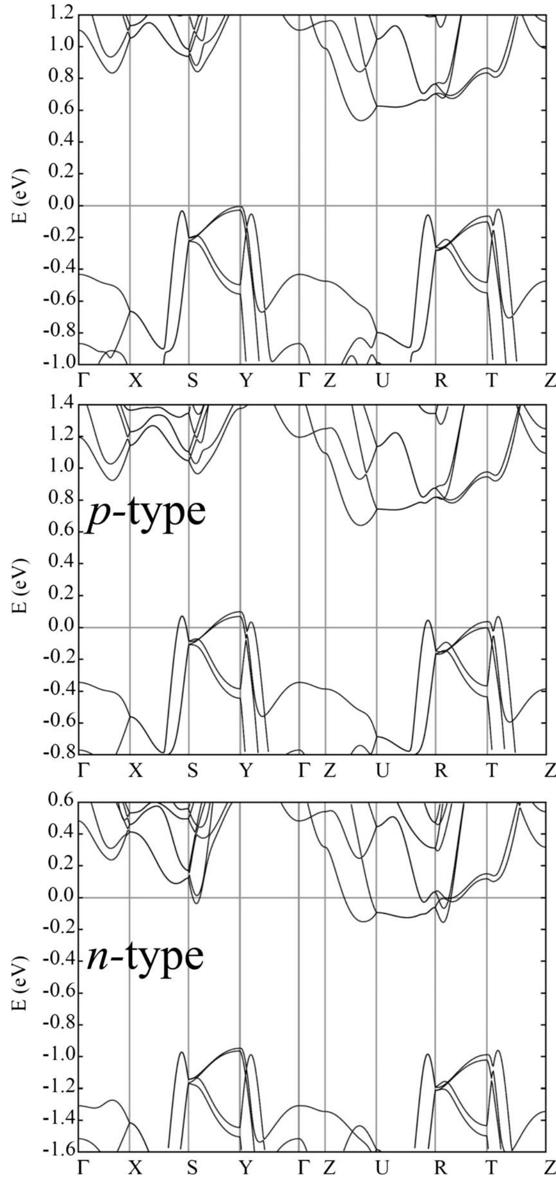

FIG. 7. Blow up of band structure near the bandgap for $(PbSe)_1(WSe_2)_1$ (top), as well as 0.1 hole/PbSe *p* doping (middle) and 0.1 electron/PbSe *n* doping (bottom) calculated with the virtual-crystal approximation. For the doped case, the energy zero is set to the Fermi level.

$$\sigma_{\alpha\beta}(i,\mathbf{k}) = e^2\tau_{i,\mathbf{k}}v_\alpha(i,\mathbf{k})v_\beta(i,\mathbf{k}), \tag{5}$$

where $\tau_{i,\mathbf{k}}$ is the scattering time and the $v_\alpha(i,\mathbf{k})$ are the components of the band velocities, $\mathbf{v}_i(\mathbf{k})=\nabla_\mathbf{k}\varepsilon_i(\mathbf{k})/\hbar$, which are obtained from the band structure. The BOLTZTRAP code does this by taking the analytic gradient of a symmetry-adapted Fourier interpolation of the band energies.[30] In this notation, the expression for the specific-heat density of states is identical to that for $\sigma_{\alpha\beta}(T,\mu)$ (Eq. (2)) except that $\sigma_{\alpha\beta}(i,\mathbf{k})$ in Eq. (4) is replaced by unity. These expressions are normally valid for metals and degenerate semiconductors, but can break down, e.g., in cases with very strong scattering, where localization may be expected, and also at very low carrier density near the Mott transition.[37–39]

All the above terms can be evaluated from the band structure except for the scattering time τ, which in general depends on temperature, doping level, and also sample details, such as defect concentrations and types. Fortunately, in many materials, while τ is a strong function of temperature and doping level, it is a weak function of energy on the scale of kT. This leads to the so-called constant scattering-time approximation, where the energy dependence of τ is neglected. We emphasize that this approximation does not rely on assumptions about the doping or T dependence of τ and is thought to be widely applicable to degenerately doped semiconductors and simple metals.[38,40] It has been successfully applied to many thermoelectric materials,[41–43] including Bi_2Te_3,[30] PbTe,[44] Na_xCoO_2,[45,46] etc. where quantitative agreement with experimental results has been shown. However, the constant scattering-time approximation is suspect in certain cases, e.g., when the electronic structure has multiple bands with different character active in transport (different scattering rates may then be expected in the different bands), and also in cases where there is a strongly energy-dependent scattering mechanism, such as in Kondo systems. The great advantage of this approximation is the exactly canceling scattering time τ in the expression of thermopower [Eq. (1)]. Thus at the fixed temperature and doping level, $S(T,\mu)$ can be directly calculated from band structures without any adjustable parameter.

As discussed above, for the case of *p*-type doping we find rigid-band behavior and so thermoelectric properties at different doping levels can be obtained using the undoped band structure with appropriate shifts of the Fermi level and furthermore the relevant bands are all derived from the PbSe layer. Accordingly, we employed the BOLTZTRAP program[30] with the band structure of the undoped compound to calculate the thermopower based on these expressions, as a function of doping level and temperature, within the constant scattering-time approximation.

We note that the out-of-plane conductivity is expected to be low, which works against thermoelectric performance, and therefore we focus on in-plane transport. We find that the orthorhombicity leads to a thermopower along the short axis, b direction, S_{yy} that is slightly larger than that in a direction (long axis), S_{xx}. Considering that we are using an approximant structure, and that in fact the films have random in-plane orientations, we present the in-plane average, $S_p = (S_{xx}+S_{yy})/2$.

Figure 8 shows the calculated in-plane average $S_p(T)$ of $(PbSe)_1(WSe_2)_1$ for various *p*-type doping levels. As may be seen, this *p*-type layered compound indeed shows high thermopowers, especially in the 300–900 K temperature range important for waste-heat recovery. This originates from heavy valence bands as mentioned. The values are higher than those of bulk PbSe with similar doping levels except at very high T (see below). For a doping level of 0.01 hole/PbSe (1.7×10^{20} cm^{-3}), the value of thermopower is above 200 μV/K in a wide temperature range (from 400 to 900 K). For the higher doping level of 0.04 hole/PbSe, $S_p(T) > 160$ μV/K is found for $T>900$ K. The decrease in thermopower at extremely high temperature at low doping is due to the minority-carrier contribution, as is often the case for low band-gap semiconductors.

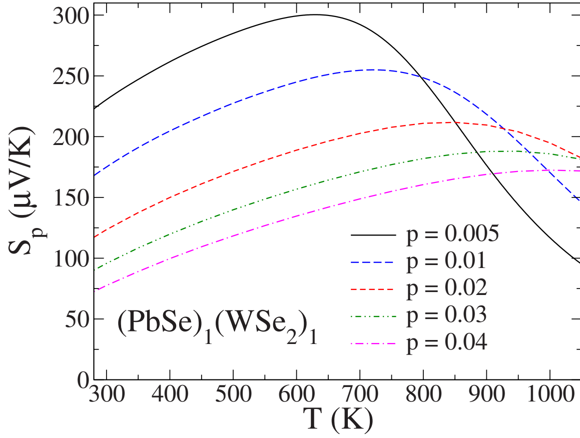

FIG. 8. (Color online) Calculated average in-plane Seebeck coefficient, S_p as a function of temperature for p-doped $(PbSe)_1(WSe_2)_1$, using the constant scattering-time approximation. The doping levels are in holes per PbSe unit.

To explore the effect of increasing the layer thickness we performed similar calculations for the $(PbSe)_2(WSe_2)_1$ system, which consists of two PbSe layers along the z direction. We did not investigate the effects of increasing the number of WSe_2 sublayers since the electronic structure near the VBM derives from the PbSe layers. The calculated thermopower of $(PbSe)_2(WSe_2)_1$ is shown in Fig. 9. The thermopower for p-doped case is qualitatively similar to $(PbSe)_1(WSe_2)_1$, the main difference being a modest decrease in the magnitudes at a roll off at lower T corresponding to the smaller band gap (see Table I). These originate from quite similar band structure to the one PbSe layer case, especially for the valence bands. In any case, although the thermopower of the two layer compound is lower than that of the one-layer compound for a fixed doping level on a per PbSe unit basis, it is still high enough to be consistent with good thermoelectric performance, especially considering that the two-layer material is expected to suffer less from interface scattering, and therefore have higher mobility. As mentioned, higher mobility means that for a given lattice thermal conductivity, $r=\kappa_e/(\kappa_l+\kappa_e)$ will be higher. In this case, the optimum ZT will be at lower carrier concentration relative to the one-layer system. As such, the lower thermopower at fixed carrier concentration may be misleading since optimizing at lower carrier concentration will work in the opposite direction, by increasing the thermopower.

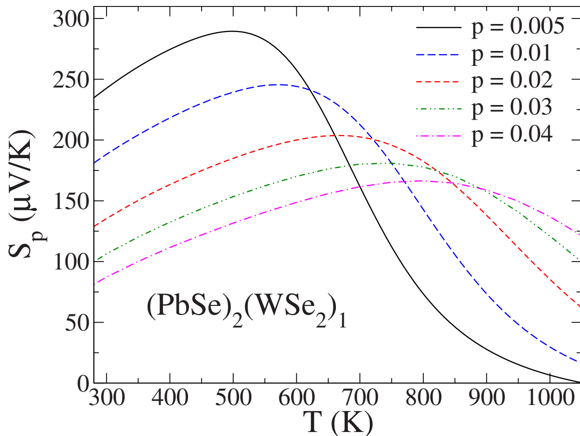

FIG. 9. (Color online) Calculated average in-plane constant scattering-time approximation Seebeck coefficient, S_p for various hole doping levels in the $(PbSe)_2(WSe_2)_1$. The doping levels are in holes per PbSe unit.

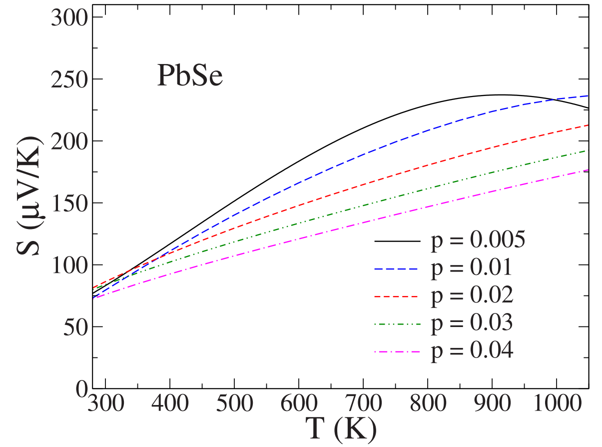

FIG. 10. (Color online) Calculated constant scattering-time approximation Seebeck coefficient, S for various hole-doping levels in cubic PbSe.

VI. RELATIONSHIP WITH PbSe

As mentioned, the structure of the valence bands for the intergrowth compounds near the VBM is similar to the band structure of PbSe, with the exception of heavier bands along k_y directions near the VBM. One may expect that as one adds more layers to the PbSe blocks in the intergrowth compounds, the electronic structure and electrical-transport properties will become more similar to those of bulk PbSe. The calculated GGA band gap is direct at the L with values of 0.32 eV in a scalar relativistic approximation and 0.07 eV with spin orbit. The experimental band gap of PbSe is 0.2 eV. Therefore both the experimental and GGA band gaps of bulk PbSe are lower than those of the intergrowth compounds. This reflects the quantum confinement of the valence bands, i.e., band narrowing due to the interfaces. Importantly, band structure (Fig. 4) is highly nonparabolic, with band velocities that actually decrease as one moves away from the VBM along the L-W line. Within a degenerately doped parabolic band model the thermopower is proportional to the effective mass (provided that T is not too high). If a forced interpretation within a parabolic band model is used, the specific nonparabolic band structure of PbSe will then yield a transport effective mass that increases with doping and also with T.

The calculated thermopower for PbSe is shown in Fig. 10. The calculations show a rather unusual temperature and doping-level dependence of the thermopower. At low temperatures, up to room temperature, the curves are inverted, i.e., the thermopower increases with increasing doping below the doping range shown. At intermediate temperatures

~300 K the curves cross and the thermopower is relatively doping independent. Then at higher temperatures, the thermopower keeps increasing up to high T, except for the lowest doping level. This is in contrast to the expected behavior for a small band-gap material, where at two sign conduction normally leads to a saturation and roll over in $S(T)$ at high T. This high-temperature behavior is consistent with experimental observations for heavily doped PbSe,[10] although direct comparison is not possible because the experimental doping levels have not been quantified. Also, even though the band gap of PbSe is lower than those in the intergrowth compounds, the high-temperature roll off does not set in until very high T. The behavior of $S(T)$ in PbSe is qualitatively similar to that of La-Te, where a combination light and heavy bands leads to a situation where a single effective-mass fit for the transport would require a doping and T-dependent effective mass.[31] Here a similar behavior arises from the nonparabolic band structure. Interestingly, for PbSe, the thermopower at a carrier concentration of 0.01 holes per formula unit is still increasing at 1100 K (note that the melting point of PbSe is ~1350 K).

Both PbSe and the intergrowth compounds show thermopowers consistent with reasonable thermoelectric performance for waste-heat recovery. The difficulty with PbSe is that the ratio r is not high enough to yield performance comparable to PbTe except at very high T. This ratio can in principle be increased by lowering the lattice thermal conductivity. Unfortunately, we are not able to obtain the scattering time τ, which controls the mobility and the thermal conductivity from the present calculations. However, based on the PbSe-dominated bands near the VBM of the intergrowth compounds, and the rigid-band behavior with doping one may speculate the intergrowth compounds behave electronically in plane similar to PbSe, at least as the PbSe layers become thicker, and that perhaps the in-plane transport properties interpolate between those of the one-layer system and those of bulk PbSe as the layer thickness is increased. Thus at some thickness one may start regarding the p-type intergrowth system as behaving like PbSe with additional boundary scattering due to the interfaces with the WSe_2 blocks. This scattering would apply to both heat-carrying phonons and to charge carriers.

To proceed we consider a case where the interface electronic scattering is strong. This is a worst case scenario for thermoelectric performance as it implies maximum degradation of the mobility by the interfaces. To mitigate this type of scattering the thickness of PbSe layers should to be larger than the effective mean-free path (MFP) of carriers in the presumably bulk PbSe-like interiors of the PbSe layers. Beyond this thickness interface scattering will not dominate the in-plane transport even if very strong. We evaluated the MFP for p-type bulk PbSe using our band-structure results and experimental-transport data. In particular, the average scattering time τ can be obtained by comparing the calculated value of σ/τ with the experimental σ. However, it is important to compare with single-crystal data for this purpose. We used the experimental data of Ref. 47 at room temperature and a doping level of 4.28×10^{18} cm^{-3} (~0.00025 holes per formula unit). This doping level is the highest for which data is available but is still considerably lower than the doping levels that we consider for thermoelectric PbSe.

In terms of Eq. (5), we can calculate the average velocity of carriers, $\bar{v}$ using $\sigma/\tau = e^2 N(\mu)\bar{v}^2$, where here $N(\mu)$ is the DOS at the Fermi level. Then the MFP, $l=\bar{v}\tau$ can be evaluated. The resulting value is ~162 Å, which is ~20 times larger than one-layer thickness of PbSe, a. Based on this, we may conclude that if thermoelectric PbSe has the same MFP as the high-mobility samples of Ref. 47, one would expect a beneficial effect due to preferential interface phonon scattering down to a thickness of ~20 layers (120 Å). If the mobility decreases significantly above ambient temperature and with doping, as seems highly likely, then the benefit due to layering will extend down to significantly lower PbSe thicknesses.

VII. SUMMARY AND CONCLUSIONS

To summarize, we used density-functional calculations and Boltzmann transport theory, to study the electronic structure and related thermoelectric properties for the misfit layered PbSe-WSe_2 materials and PbSe. Starting from the prototype $(PbSe)_1(WSe_2)_1$, we find it is a semiconductor with the indirect bandgap of 0.43 eV, where the edge of valence bands is mainly dominated by PbSe sublattice. The band gap decreases with PbSe thickness. In both the intergrowth compounds and in bulk PbSe the band-structure contributions to transport cannot be described in a simple single-parabolic band picture. Instead the thermopower is enhanced by the heavy-band features. In bulk PbSe this leads to an increase in the high-temperature thermopower, which is consistent with the fact that the best ZT values for PbSe are at high temperature where it can have better performance than PbTe.[10] We find that high thermopowers consistent with good thermoelectric performance occur up to high doping levels of 0.01–0.02 holes per formula unit for T in the range 300–900 K for the one- and two-layer compounds but somewhat lower values of the doping level for PbSe.

The present results suggest that it may be possible to optimize the WSe_2-PbSe intergrowth compounds for high thermoelectric performance at temperatures appropriate for waste-heat recovery. This material, grown by techniques, may not be directly suitable for waste-heat-recovery applications where cost is important. However, a finding of high ZT in the appropriate temperature range in this material would show that nanostructured PbSe can be a high ZT material perhaps leading to the discovery of bulk materials based on this principle.

ACKNOWLEDGMENTS

We are grateful to M.H. Du for helpful discussions and to David Johnson and Qiyin Lin for helpful discussions and for making available republications data. The crystal-structure figure was produced with the XCRYSDEN program.[48] This work was supported by the Department of Energy, Vehicle Technologies, Propulsion Materials Program, the ORNL LDRD program, and the S3TEC EFRC.

[1] J. Yang, in *Proceedings of the 24th International Conference on Thermoelectrics* (IEEE, Piscataway, 2005), p. 170.
[2] G. J. Snyder and E. S. Toberer, Nature Mater. **7**, 105 (2008).
[3] L. E. Bell, Science **321**, 1457 (2008).
[4] A. F. Ioffe, *Semiconductor Thermoelements and Thermoelectric Cooling* (Inforsearch, London, 1957).
[5] C. Wood, Rep. Prog. Phys. **51**, 459 (1988).
[6] K. F. Hsu, S. Loo, F. Guo, W. Chen, J. S. Dyck, C. Uher, T. Hogan, E. K. Polychroniadis, and M. G. Kanatzidis, Science **303**, 818 (2004).
[7] J. P. Heremans, V. Jovovic, E. S. Toberer, A. Saramat, K. Kurosaki, A. Charoenphakdee, S. Yamanaka, and G. J. Snyder, Science **321**, 554 (2008).
[8] D. M. Rowe, *CRC Handbook of Thermoelectrics* (CRC, Boca Raton, 1995).
[9] J. An, A. Subedi, and D. J. Singh, Solid State Commun. **148**, 417 (2008).
[10] G. T. Alekseeva, E. A. Gurieva, P. P. Konstantinov, L. V. Prokofeva, and M. I. Fedorov, Semiconductors **30**, 1125 (1996) [Fiz. Tekh. Poluprovodn. **30**, 2159 (1996)].
[11] H. Abrams and R. N. Tauber, J. Appl. Phys. **40**, 3868 (1969).
[12] G. A. Slack, *CRC Handbook of Thermoelectrics* (CRC, Boca Raton, Florida, 1995), pp. 407–440
[13] B. C. Sales, D. Mandrus, and R. K. Williams, Science **272**, 1325 (1996).
[14] T. C. Harman, P. J. Taylor, M. P. Walsh, and B. E. LaForge, Science **297**, 2229 (2002).
[15] B. Poudel, Q. Hao, Y. Ma, Y. Lan, A. Minnich, B. Yu, X. Yan, D. Wang, A. Muto, D. Vashaee, Xiaoyuan Chen, Junming Liu, Mildred S. Dresselhaus, Gang Chen, and Zhifeng Ren, Science **320**, 634 (2008).
[16] H. Beyer, J. Nurnus, H. Böttner, A. Lambrecht, E. Wagner, and G. Bauer, Physica E **13**, 965 (2002).
[17] R. Y. Wang, J. P. Feser, J. S. Lee, D. V. Talapin, R. Segalman, and A. Majumdar, Nano Lett. **8**, 2283 (2008).
[18] C. Chiritescu, D. G. Cahill, N. Nguyen, D. Johnson, A. Bodapati, P. Keblinski, and P. Zschack, Science **315**, 351 (2007).
[19] Q. Lin, C. L. Heideman, N. Nguyen, P. Zschack, C. Chiritescu, D. G. Cahill, and D. C. Johnson, Eur. J. Inorg. Chem. **2008**, 2382 (2008).
[20] C. Chiritescu, D. G. Cahill, C. Heideman, Q. Lin, C. Mortensen, N. T. Nguyen, D. Johnson, R. Rostek, and H. Böttner, J. Appl. Phys. **104**, 033533 (2008).
[21] Qiyin Lin and David C. Johnson (unpublished).
[22] A. Mavrokefalos, N. T. Nguyen, M. T. Pettes, D. C. Johnson, and L. Shi, Appl. Phys. Lett. **91**, 171912 (2007).
[23] W. J. Schutte, J. L. De Boer, and F. Jellinek, J. Solid State Chem. **70**, 207 (1987).
[24] J. Rouxel, A. Meerschaut, and G. A. Wiegers, J. Alloys Compd. **229**, 144 (1995).
[25] J. P. Perdew, K. Burke, and M. Ernzerhof, Phys. Rev. Lett. **77**, 3865 (1996).
[26] G. Kresse and D. Joubert, Phys. Rev. B **59**, 1758 (1999).
[27] G. Kresse and J. Furthmüller, Phys. Rev. B **54**, 11169 (1996).
[28] D. J. Singh and L. Nordstrom, *Planewaves Pseudopotentials and the LAPW Method*, 2nd ed. (Springer, Berlin, 2006).
[29] P. Blaha, K. Schwarz, G. Madsen, D. Kvasnicka, and J. Luitz, WIEN2K, *An Augmented Plane Wave + Local Orbitals Program for Calculating Crystal Properties* (K. Schwarz, Tech. Univ. Wien, Austria, 2001).
[30] G. K. H. Madsen and D. J. Singh, Comput. Phys. Commun. **175**, 67 (2006).
[31] A. F. May, D. J. Singh, and G. J. Snyder, Phys. Rev. B **79**, 153101 (2009).
[32] D. J. Singh and I. I. Mazin, Phys. Rev. B **56**, R1650 (1997).
[33] L. D. Hicks and M. S. Dresselhaus, Phys. Rev. B **47**, 12727 (1993).
[34] E. A. Albanesi, C. M. I. Okoye, C. O. Rodriguez, E. L. Peltzer y Blanca, and A. G. Petukhov, Phys. Rev. B **61**, 16589 (2000).
[35] R. Coehoorn, C. Haas, J. Dijkstra, C. J. F. Flipse, R. A. de Groot, and A. Wold, Phys. Rev. B **35**, 6195 (1987).
[36] S. Sharma, C. Ambrosch-Draxl, M. A. Khan, P. Blaha, and S. Auluck, Phys. Rev. B **60**, 8610 (1999).
[37] J. M. Ziman, *Electrons and Phonons* (Oxford University Press, New York, 2001).
[38] W. Jones and N. H. March, *Theoretical Solid State Physics* (Courier Dover, New York, 1985).
[39] P. A. Lee and T. V. Ramakrishnan, Rev. Mod. Phys. **57**, 287 (1985).
[40] J. B. Smith and H. Ehrenreich, Phys. Rev. B **25**, 923 (1982).
[41] D. J. Singh, *Semiconductors and Semimetals*, Thermoelectric Materials Research, Vol. 70 (Academic, New York, 2000).
[42] L. Bertini and C. Gatti, J. Chem. Phys. **121**, 8983 (2004).
[43] L. Lykke, B. B. Iversen, and G. K. H. Madsen, Phys. Rev. B **73**, 195121 (2006).
[44] Y. Wang, X. Chen, T. Cui, Y. Niu, Y. Wang, M. Wang, Y. Ma, and G. Zou, Phys. Rev. B **76**, 155127 (2007).
[45] D. J. Singh and D. Kasinathan, J. Electron. Mater. **36**, 736 (2007).
[46] H. J. Xiang and D. J. Singh, Phys. Rev. B **76**, 195111 (2007).
[47] R. S. Allgaier and W. W. Scanlon, Phys. Rev. **111**, 1029 (1958).
[48] A. Kokalj, J. Mol. Graphics Modell. **17**, 176 (1999).